



PII S0016-7037(98)00130-6

PAUL GAST LECTURE

Geochemical and geophysical implications of the radiocarbon calibration

EDOUARD BARD*

CEREGE, Université Aix-Marseille III and CNRS, Institut Universitaire de France,
Europôle de l'Arbois, 13545, Aix-en-Provence cedex 4, France

(Received March 10, 1998; accepted in revised form March 10, 1998)

Abstract—A precise and accurate chronological framework is crucial to study the dynamics of a variety of phenomena which occurred during the last 45,000 years. Although the ^{14}C dating method has been widely applied since the 1950s, it is recognized that the atmospheric $^{14}\text{C}/^{12}\text{C}$ ratio has not been stable during the past. In order to calculate accurate ages, these fluctuations have to be corrected by means of a calibration curve obtained by comparing raw ^{14}C measurements with true calendar ages provided by independent dating methods.

The calibration curve obtained so far is characterized by a long-term trend with raw ^{14}C ages being significantly younger than calendar ages during most of the last 45,000 years. Abrupt ^{14}C shifts, which occurred over centuries to millennia, are superimposed on this long-term trend of decreasing atmospheric $^{14}\text{C}/^{12}\text{C}$ ratio. To a certain extent, it is possible to outline the different causes of atmospheric ^{14}C variations by considering complementary information obtained from other cosmogenic nuclides studied at different latitudes: (1) Most high-frequency changes in the atmospheric $^{14}\text{C}/^{12}\text{C}$ ratio are linked to magnetic fluctuations of solar origin as revealed by studying the last three centuries for which direct observations of the Sun are available. A similar conclusion is derived by comparing $^{14}\text{C}/^{12}\text{C}$ events with ^{10}Be and ^{36}Cl concentration maxima in polar ice cores. (2) The long-term trend shift of ^{14}C ages is due to a long period of decreased shielding effect of the geomagnetic dipole field which occurred over the interval between 10,000 and 40,000 years BP. This interpretation is supported by paleomagnetic measurements performed on volcanic and sedimentary rocks and by ^{10}Be and ^{36}Cl analysed in low and high latitude records. (3) A prominent and rapid atmospheric $^{14}\text{C}/^{12}\text{C}$ excursion occurred between 13,000 and 11,500 cal-yr-BP, thus corresponding to the Younger Dryas cold period. By contrast with the ^{14}C variability mentioned above, which is linked to ^{14}C production changes, this so-called ^{14}C age plateau is probably due to an abrupt variation in the rates of exchange within the global carbon cycle. This interpretation is supported by independent geochemical proxies and by numerical modelling of the carbon cycle. Copyright © 1998 Elsevier Science Ltd

1. INTRODUCTION

The radiocarbon dating method, for which Willard Libby obtained the Nobel Prize for Chemistry in 1960, is based on the beta decay of ^{14}C atoms originally produced in the upper atmosphere by secondary neutrons generated by cosmic-ray protons (Libby, 1952).

This method has been widely used to date samples up to 45,000 years old and has provided a precise chronological framework for several scientific fields. For example, the ^{14}C method has been crucial in prehistoric archeology for studying the spread and development of populations during the paleolithic and neolithic periods. In geophysics, the ^{14}C method is important in establishing recurrence times of earthquakes or volcanic eruptions.

The field of paleoclimatology clearly illustrates the importance of the ^{14}C method and the need for both precision and accuracy. Indeed, rapid climatic changes are studied in different types of records spread over different latitudes and in

different compartments of the ocean-atmosphere-biosphere system. The accuracy of ^{14}C dating is also crucial in evaluating the correlation between climatic events and variations in the Earth's orbital parameters calculated by astronomers.

Unlike most other radiochronological methods (U-Th, Rb-Sr, Sm-Nd, K-Ar, Lu-Hf, Re-Os, etc.), it is unfortunately not possible to measure the ratio between the parent isotope, ^{14}C , and its daughter product, radiogenic ^{14}N , which is indistinguishable from common nitrogen. The ^{14}C method is nonetheless accurate, but the initial $^{14}\text{C}/^{12}\text{C}$ ratio of the sample has to be known in order to calculate a true calendar age. Most samples dated by ^{14}C have extracted their carbon directly from the atmosphere (e.g., plant remains) or indirectly through the food chain (e.g., animal remains). The calibration problem thus consists of evaluating the past variations of the atmospheric $^{14}\text{C}/^{12}\text{C}$ ratio which is very sensitive to production changes and, to a lesser degree, to rearrangements within the global carbon cycle.

2. MATERIALS AND METHODS

Several ways have been devised to reconstruct past fluctuations of the atmospheric $^{14}\text{C}/^{12}\text{C}$ ratio by comparing ^{14}C mea-

*This paper is the first Paul Gast Lecture delivered June 2, 1997, during the Seventh Annual V. M. Goldschmidt Conference held in Tucson, Arizona, USA.

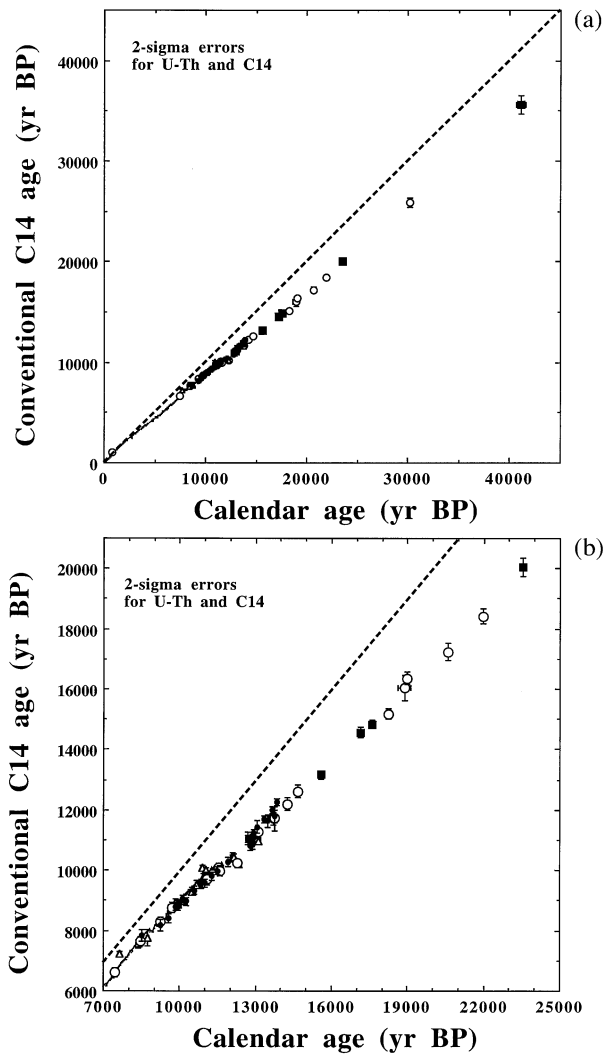


Fig. 1. (a) AMS-¹⁴C ages plotted vs. TIMS-²³⁰Th ages obtained on corals. Statistical errors for coral ages are quoted at the 2σ level. Open dots represent the data from Barbados, black dots the data from Tahiti, the four youngest black squares the data from Mururoa (Bard et al., 1990, 1993, 1996, and 1998) and open triangles and the oldest black square the data from New-Guinea (Edwards et al., 1993; Bard et al., 1998). The thin wiggly curve is the smoothed tree-ring calibration and the dashed line is the 1:1 correlation line. For ages beyond the Younger-Dryas/Preboreal boundary (10,000 ¹⁴C-yr-BP) the coral data can be approximated by a simple linear equation: $[\text{Age cal-yr-BP}] = 1.168 \times [\text{Age } ^{14}\text{C-yr-BP}]$, or even better by a second order polynomial: $[\text{Age cal-yr-BP}] = -3.0126 \times 10^{-6} \times [\text{Age } ^{14}\text{C-yr-BP}]^2 + 1.2896 \times [\text{Age } ^{14}\text{C-yr-BP}] - 1005$. (b) Detail of Fig. 1a: AMS-¹⁴C ages plotted vs. TIMS-²³⁰Th ages obtained on corals.

measurements with true ages measured in the same samples using an independent dating technique (Fig. 1a,b). For the Holocene period (ca. the last 10,000 yr) it has been possible to find abundant fossil pines and oaks and thus produce a high-resolution atmospheric ¹⁴C/¹²C curve by comparing ¹⁴C levels and tree ring counts on the same tree logs (Stuiver et al., 1986; Kromer and Becker, 1993; Kromer and Spurk, 1998). Unfortunately, it has not been possible to pursue this so-called dendrocalibration much further because of the scarcity of

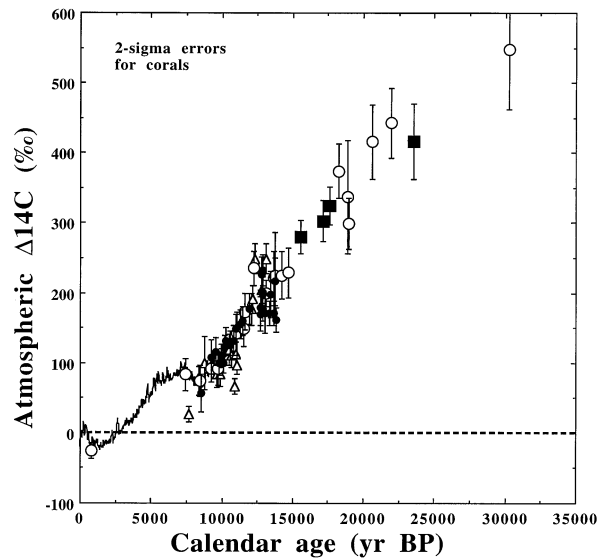


Fig. 2. Atmospheric $\Delta^{14}\text{C}$ vs. time as calculated by using the AMS-¹⁴C ages vs. TIMS-²³⁰Th comparison (Fig. 1). Statistical errors for coral data are quoted at the 2σ level. Open dots represent the data from Barbados, black dots the data from Tahiti, black squares the data from Mururoa (Bard et al., 1990, 1993, 1996 and 1998) and open triangles the data from New Guinea (Edwards et al., 1993).

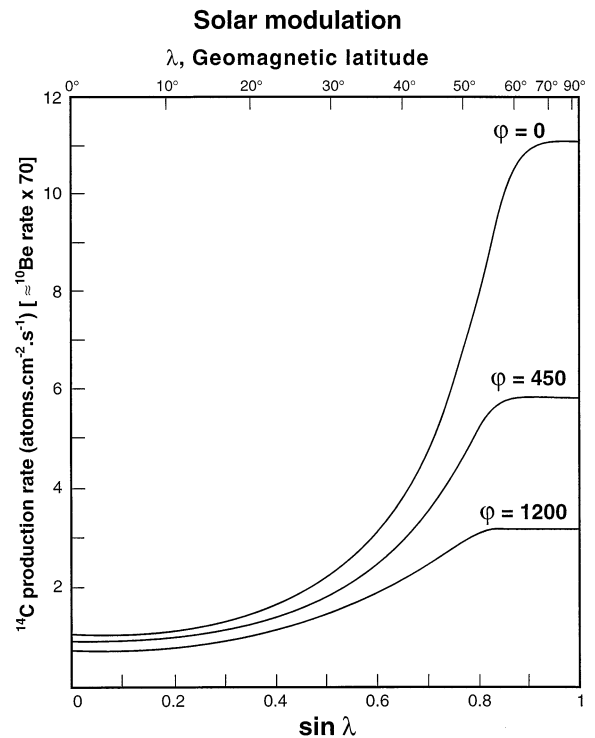


Fig. 3. ¹⁴C production rates calculated as a function of geomagnetic latitude and for different values of the solar modulation parameter ϕ (after Lal, 1988). Note that typical solar-minimum and -maximum ϕ values are 300 and 900, respectively, and that 450 is the average effective value during a typical 11-yr solar cycle. ¹⁰Be production rates can be approximated by dividing all ¹⁴C values by a constant factor of 70 which corresponds to the ratio of ¹⁴C (Lal, 1988) and ¹⁰Be global productions (Monaghan et al., 1985).

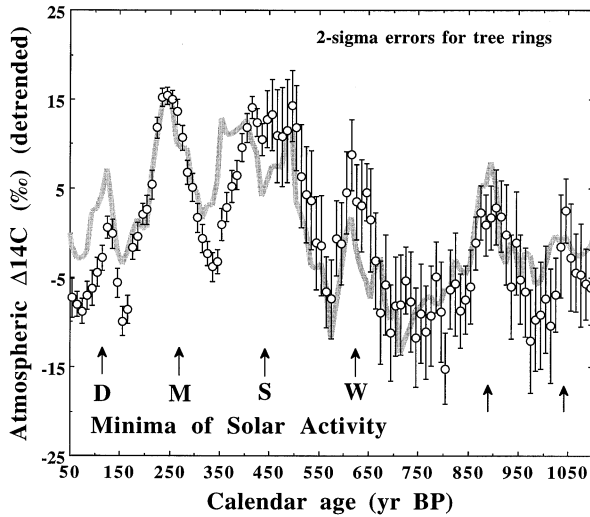


Fig. 4. Open dots represent the detrended $\Delta^{14}\text{C}$ values measured in American and European tree rings (Stuiver and Reimer, 1993). These measurements have been corrected for the long term trend visible in Fig. 2 (ca. 10‰ over the last millennium). As explained in the text, this trend is probably due to the memory of long-term geomagnetic variations. The grey curve represents the tropospheric $\Delta^{14}\text{C}$ variations simulated by using relative changes of ^{10}Be at the South Pole as an input curve to a twelve-box carbon cycle model (see Bard et al., 1997 for details of calculations). Note that the ^{10}Be -based $\Delta^{14}\text{C}$ variations closely resemble the ^{14}C measurements obtained on tree rings ($R=0.81$). In particular, it is easy to identify periods of maximal $\Delta^{14}\text{C}$ which correspond to solar activity minima (vertical arrows) centred at about 120 yr BP (Dalton), 260 yr BP (Maunder), 450 yr BP (Spörer), 630 yr BP (Wolf), 890 and 1040 yr BP.

trees during the late Pleistocene which was characterized by an extreme glacial climate. Other types of records have thus been used to continue the calibration effort: annually laminated sediments (Goslar et al., 1995; Hughen et al., 1998; Kitagawa and van der Plicht, 1998) and shallow corals from tropical islands which can be cross-dated by high-precision ^{14}C and $^{230}\text{Th}/^{234}\text{U}$ dating by means of mass spectrometric

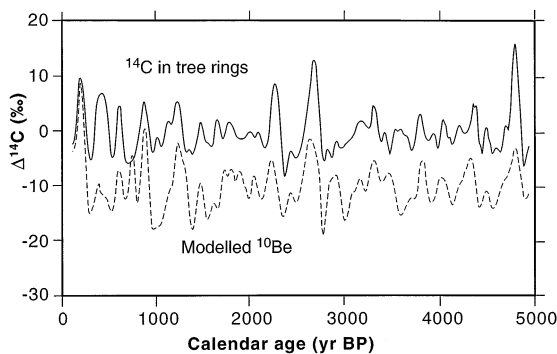


Fig. 5. The upper curve represents the measured $\Delta^{14}\text{C}$ in tree ring after removal of the long-term trend by a high-pass filter. The lower dotted curve shows calculated $\Delta^{14}\text{C}$ based on ^{10}Be data measured in Greenland ice cores (Camp Century and Milcent; see Beer et al., 1988 for details on the data and model calculations). The lower curve is shifted by 10‰ for easier comparison. Note the correlation between both time series ($R = 0.58$). After Beer et al., 1988.

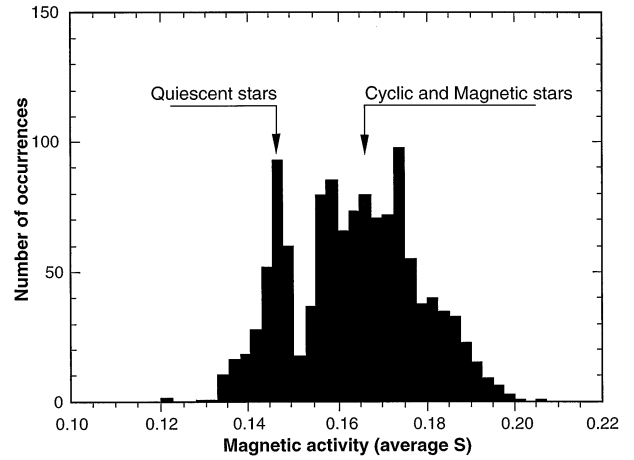


Fig. 6. Frequency distribution of magnetic activity in seventy-four solar-type stars. The stellar magnetic activity S corresponds to the time-averaged value of the relative calcium H and K flux measured by reflectors at the Mount Wilson Observatory. The broad peak at higher values of magnetic activity ($S > 0.15$) corresponds to the broad distribution expected for stars varying periodically and observed at random phases in their cycles. The narrow peak at low values of ($S < 0.15$) may represent stars sampled in Maunder minima. After Baliunas and Jastrow (1990).

techniques (Bard et al., 1990a, 1993, 1996, 1998; Edwards et al., 1993).

The use of corals has been boosted by the development of mass spectrometric techniques which enable the dating of much smaller samples and which yield better precisions than traditional techniques of radioactivity counting (beta for ^{14}C and alpha for $^{230}\text{Th}/^{234}\text{U}$). Accelerator mass spectrometry was developed in the 1970s to determine $^{14}\text{C}/^{12}\text{C}$ ratios in natural samples ranging between 10^{-12} and 10^{-15} (Nelson et al., 1977; Bennett et al., 1977). Since the 1980s, this revolutionary technique has been used to date milligram-sized carbon samples, thus allowing thorough screening and cleaning of biogenic carbonates (Andree et al., 1984; Broecker et al., 1984; Dup-

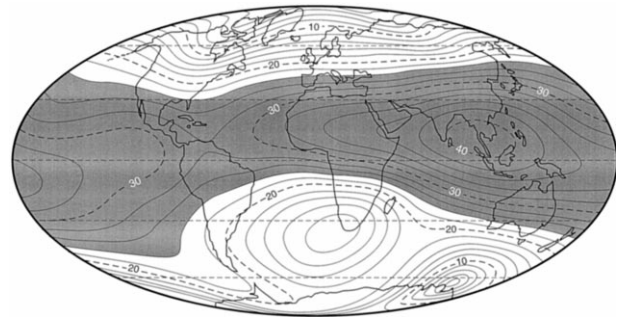


Fig. 7. International Geomagnetic Reference Field (IGRF, 1990) for the horizontal field component H expressed in 10^3 gamma units (after a figure from USGS in Campbell, 1997). Cosmic-ray protons with a vertical incidence are strongly deflected by this horizontal component. This figure clearly shows that the horizontal component of the magnetic force will be at maximum for low latitudes (shaded zone) and at minimum for high latitudes. This effect is responsible for the strong dependence of ^{14}C and ^{10}Be productions vs. geomagnetic latitude illustrated on Fig. 3.

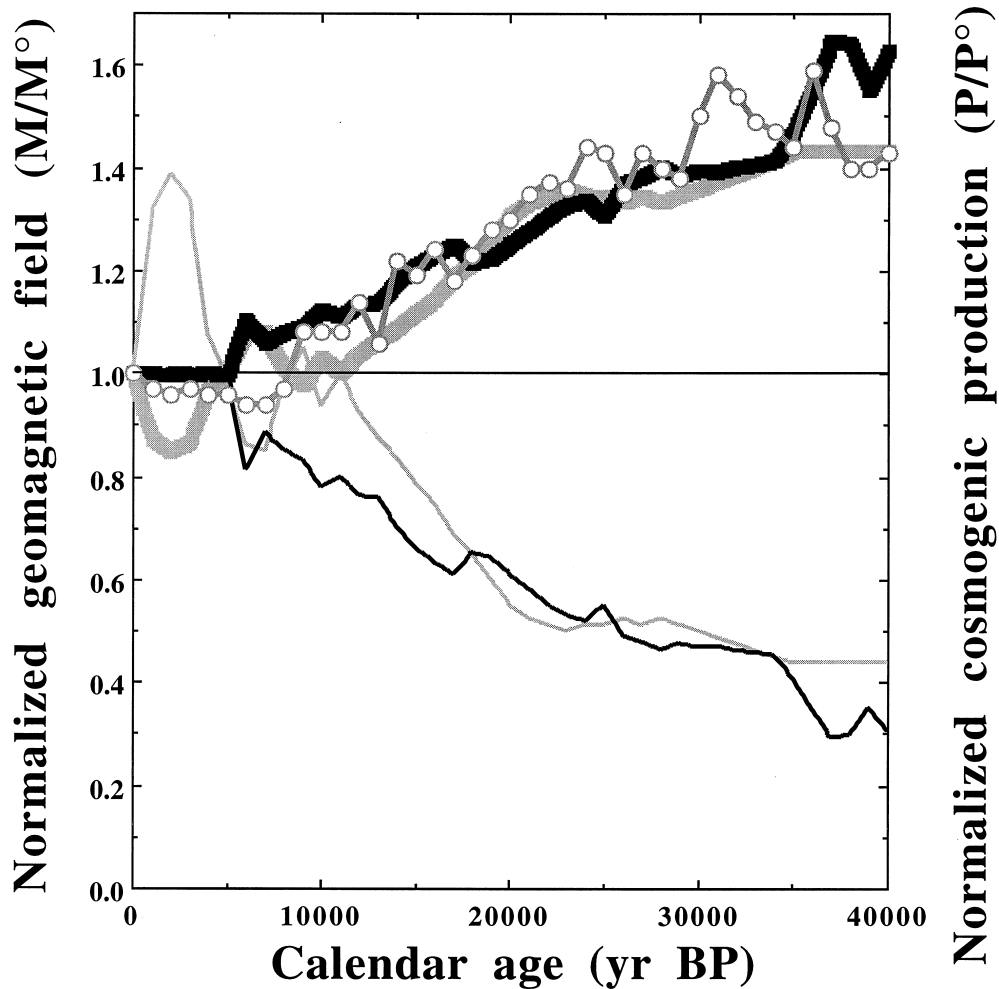


Fig. 8. Geomagnetic intensity and cosmogenic nuclide production during the last 40,000 cal-yr-BP. Thin curves are associated with the left-hand y-axis and represent the intensity of Earth's magnetic dipole (M) normalized to the present-day value (M°). The thin grey curve is a fit through data measured on volcanic rocks and compiled by McElhinny and Senanayake (1982). The thin black curve shows the compilation by Guyodo and Valet (1996) which is based on relative geomagnetic intensities measured in marine sediments from all oceanic basins. Thick curves are associated with the right-hand y-axis and represent the global cosmogenic production (P) normalized to the present-day value (P°). The thick grey and black curves are inferred from the two paleomagnetic time-series (thin grey and black curves, respectively) and theoretical calculations by Lal (1988) shown in Fig. 9. The grey curve with open dots shows the global ^{10}Be flux during the past 40,000 yr compiled recently by Frank et al. (1997). This record is in good agreement with the theoretical predictions based on both paleomagnetic records.

lessy et al., 1986; Bard et al., 1987). The same principle, counting atoms instead of waiting for them to decay, was applied in the 1980s for the development of $^{234}\text{U}/^{230}\text{Th}$ dating by thermal ionization mass spectrometry (Edwards et al., 1987). Modern mass spectrometers equipped with ion-counting detectors make it possible to obtain 2σ errors of 20–60 years for ^{230}Th ages ranging from 8,000 to 14,000 yr BP (Edwards et al., 1993; Bard et al., 1996; BP stands for before present, present being taken as the year 1950).

Altogether, the different calibration methods led to the reconstruction of significant variations of the atmospheric $^{14}\text{C}/^{12}\text{C}$ ratio through time usually expressed as a deviation from

the present day ratio: i.e., $\Delta^{14}\text{C}$ in terms of ‰ (Broecker and Olson, 1961; Stuiver and Polach, 1977). Figure 2 compiles the updated tree-ring data (Kromer and Spurk, 1998) and coral data from Barbados, Mururoa, Tahiti (Bard et al., 1993, 1996, 1998), and New-Guinea (Edwards et al., 1993). This $\Delta^{14}\text{C}$ record indicates clearly that the atmospheric $\Delta^{14}\text{C}$ was about 400–500‰ higher between about 20,000 and 30,000 yr BP and that it essentially decreased between 18,000 and 3000 yr BP. As shown by high-resolution studies based on ^{14}C in tree rings, there are also numerous high-frequency peaks, with durations of the order of a few centuries, which are superimposed on the long-term decreasing trend.

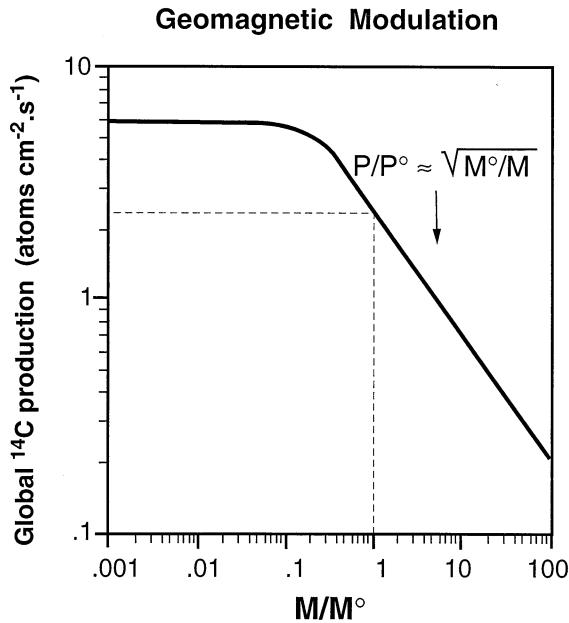


Fig. 9. Global ^{14}C production as a function of the intensity of Earth's magnetic dipole (data from Lal, 1988; the present day production is $2.72 \text{ }^{14}\text{C} \text{ atoms.cm}^{-2} \cdot \text{s}^{-1}$). Note that the shielding effect levels off at low values below 20% of the present geomagnetic dipole. Above this threshold, the log of the ^{14}C production is negatively correlated to the log of M/M^0 with a slope of about -0.5 . This corresponds to the simple formula $P/P^0 = (M/M^0)^{-1/2}$ derived by Elsasser et al. (1956).

Besides its fundamental use for radiocarbon dating, the atmospheric $\Delta^{14}\text{C}$ curve provides abundant information on a variety of geophysical, geochemical, and even astronomical phenomena.

2.1. The High-Frequency Component

As first shown by Stuiver (1961), the rapid excursions observed during the Holocene are linked to century-scale fluctuations of the solar magnetic activity similar to the so-called Maunder Minimum period of the late 17th century, during which sunspots were almost absent (deMairan 1733; Maunder 1894). Similarly, all periods of low sunspot occurrence over the last four centuries are characterized by high $\Delta^{14}\text{C}$ values (Eddy, 1976; Stuiver and Quay, 1980).

A way of checking the solar origin of the $\Delta^{14}\text{C}$ wiggles is to compare these fluctuations with an independent record based on other cosmogenic radionuclides such as ^{10}Be measured in polar ice (Raisbeck et al., 1981). However, ^{14}C and ^{10}Be time series cannot be compared directly since the fates of these two cosmogenic nuclides are very different after their production in the atmosphere: ^{10}Be becomes fixed to aerosols and is washed out by precipitation in a matter of a year. ^{10}Be fallout is thus a marker of the regional, latitude-dependant, cosmogenic production (Fig. 3). By contrast, ^{14}C is oxidized and homogenized in the atmospheric $^{12}\text{CO}_2$ pool which is connected to larger reservoirs of the carbon cycle such as the biosphere and bicarbonate dissolved in the oceans. Atmospheric $\Delta^{14}\text{C}$ thus follows the average global production, but short-term variations are

strongly damped by the carbon cycle. The use of a mathematical model is required to quantify this inherent bias (Craig, 1956; deVries, 1958; Oeschger et al., 1975; Siegenthaler et al., 1980).

The relative fluctuations of ^{10}Be concentrations measured in the South Pole ice record were recently used as an input to a twelve-box numerical model to convert the data into a synthetic $\Delta^{14}\text{C}$ record (Bard et al., 1997). On Fig. 4, the modelled curve is compared with the decadal ^{14}C data measured in tree rings. It is easy to identify periods of maximum $\Delta^{14}\text{C}$ which correspond to solar activity minima centred at about 120 yr BP (Dalton), 260 yr BP (Maunder), 450 yr BP (Spörer), 630 yr BP (Wolf), 890 and 1040 yr BP. Cross correlation calculations suggest that there is no significant lag between the ^{10}Be -based $\Delta^{14}\text{C}$ and the measured tree-ring $\Delta^{14}\text{C}$ records. This study confirms the dominance of solar modulation on the variations of cosmogenic production over the last millenium.

Similar analyses of the tree-ring $\Delta^{14}\text{C}$ and Greenland ice ^{10}Be and ^{36}Cl records were performed for the last 5,000 years (Beer et al., 1988; Finkel and Nishiizumi, 1996). As illustrated on Fig. 5, these studies revealed that the Sun has spent roughly a third of its recent history in magnetic minima that are equivalent to the Maunder minimum. Statistical analyses by astronomers (Baliunas and Jastrow, 1990; Lockwood et al., 1992) suggest that this is indeed a typical behaviour for solar-type stars (Fig. 6).

The concomitant variations of the ^{14}C , ^{10}Be , and ^{36}Cl productions could ultimately be used as proxies for the solar irradiance provided that astrophysicists and solar dynamicists improve their knowledge of the relationship between star brightness and magnetic activity (Zhang et al., 1994). Furthermore ^{14}C , ^{10}Be , and ^{36}Cl data may provide additional climatic information if a direct link between cosmic rays, water vapour condensation, and cloud cover is confirmed (Tinsley, 1994; Svensmark and Friis-Christensen, 1997).

3.2. The Long-Term Trend between 30,000 and 3000 cal-yr-B

By contrast, the long-term 400–500% decrease in the atmospheric $\Delta^{14}\text{C}$ ratio cannot be explained by magnetic fluctuations of the Sun. One major argument for this conclusion comes from the variations observed for ^{10}Be and ^{36}Cl measured in records spread over different latitudes. Due to its orientation (see Fig. 7), the geomagnetic field acts as a shield against primary cosmic-ray protons mainly at low and mid latitudes (Fig. 3). ^{14}C , being rapidly mixed in the atmospheric CO_2 reservoir, loses its latitudinal dependence. This is not the case for ^{10}Be and ^{36}Cl , which are mainly modulated between 60°S and 60°N .

A broad picture tends to emerge from several studies of ^{10}Be and ^{36}Cl fluxes in polar ice and other records: a long-term decrease during the last 30,000 yr is present in low and mid latitudes ^{10}Be and ^{36}Cl records (Lao et al., 1992; Frank et al., 1997; Plummer et al., 1997) but, by contrast, this is essentially absent in polar profiles (Raisbeck et al., 1992; Yiou et al., 1998; Finkel and Nishiizumi, 1996, 1998). These observations strongly suggest that the long-term decrease of cosmogenic production is a response to a slow change of the global geomagnetic dipole.

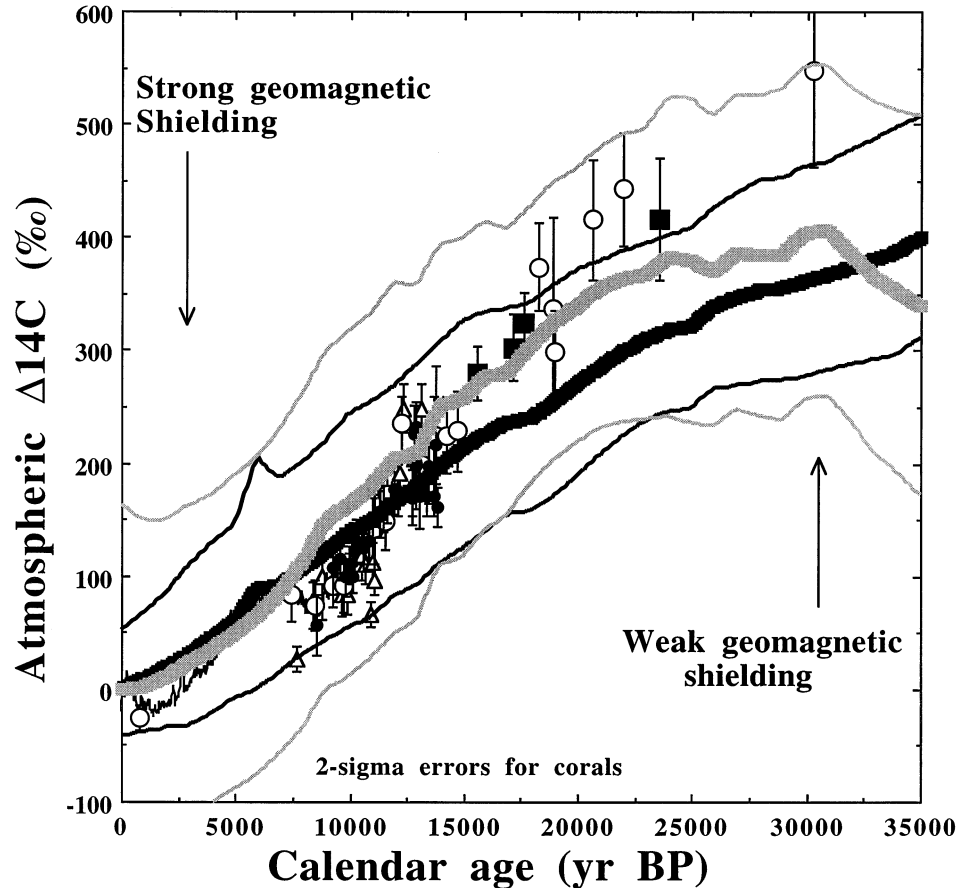


Fig. 10. Atmospheric $\Delta^{14}\text{C}$ vs. time as calculated by using the AMS- ^{14}C ages vs. TMS- ^{230}Th ages comparison. Statistical errors for coral data are quoted at the 2σ level. Open dots represent the data from Barbados, black dots the data from Tahiti, black squares the data from Mururoa (Bard et al., 1990, 1993, 1996 and 1998) and open triangles the data from New Guinea (Edwards et al., 1993). The thick black and grey lines correspond, respectively, to the $\Delta^{14}\text{C}$ expected from past changes of the cosmnuclide production as derived from paleomagnetic data by Guyodo and Valet (1996) and from global ^{10}Be flux by Frank et al. (1997). For these calculations, the production curves shown in Fig. 8 were used as inputs for a simple carbon cycle box-model used in Bard et al. (1990). The thin black and grey lines correspond to 2σ errors on these calculations, taking into account the scatter of the compiled records of geomagnetic intensity and global ^{10}Be flux.

Paleomagneticians have been able independently to reconstruct past variations of the geodynamo strength by studying volcanic rocks, lacustrine and marine sediments (McElhinny and Senanayake, 1982; Tric et al., 1992; Thouveny et al., 1993; Tauxe, 1993). As compiled recently by Guyodo and Valet (1996) the deep-sea sediment record is mainly characterized by a twofold increase of the geomagnetic field during the period between 30,000 and 5,000 yr BP (Fig. 8). By using calculations of Lal (1988; Fig. 9), these paleomagnetic records can then be used to make theoretical predictions of cosmnuclide production through time which must have been significantly enhanced during periods of weak magnetic shielding. In order to make a comparison with the $\Delta^{14}\text{C}$ data, it is again necessary to take into account the secondary effect of ^{14}C mixing within the global carbon cycle which slightly smoothes fast changes and introduces a delay and a memory effect into the system. The resulting $\Delta^{14}\text{C}$ records (Fig. 10) suggest that a significant part of the 400–500‰ decrease based on corals data can be accounted for by an increase of the geomagnetic field.

The global ^{10}Be flux record compiled from marine sediments by Frank et al. (1997) is in very good agreement with the theoretical predictions based on the paleomagnetic variations (Fig. 8). Comparing this ^{10}Be record with the $\Delta^{14}\text{C}$ data reinforces the conclusion that the long-term decrease of the atmospheric $\Delta^{14}\text{C}$ is due to a long-term increase of the geomagnetic field (Fig. 10).

Between 20,000 and 30,000 yr BP, it seems that the atmospheric $\Delta^{14}\text{C}$ data measured on corals are slightly higher than the model results based on the paleomagnetic and ^{10}Be records. Nevertheless, these modelled curves are not yet precise enough to really be sure that the difference is significant (see uncertainties on Fig. 10). In addition, the paleomagnetic intensity and ^{10}Be flux records could suffer from natural smoothing due to several causes such as the stacking procedure, bioturbation phenomena, and the fact that high-latitude sediments are under-represented in the published compilations. Furthermore, this 20,000–30,000 cal-yr-BP interval corresponds to the last glacial period during which major changes affected the carbon cycle

and hence the atmospheric $\Delta^{14}\text{C}$ (Fig. 11). For example, studies of air bubbles enclosed in old polar ice show that the atmospheric CO_2 concentration was 30% lower during the glacial period than during the Holocene (Delmas et al., 1980; Neftel et al., 1982). During this glacial period, the global biosphere reservoir was also reduced (Adams et al., 1990; Van Campo et al., 1993; Crowley, 1995) and the penetration rate of $^{14}\text{CO}_2$ into the deep ocean was significantly diminished in response to a sluggish thermohaline circulation (Broecker et al., 1990) and the presence of widespread sea-ice at high-latitudes. Numerical model calculations (e.g., Fig. 11) combined with other paleo-data suggest that the total effect of carbon cycle changes could account for about a 100‰ additional increase in the atmospheric $\Delta^{14}\text{C}$, in rough agreement with the $\Delta^{14}\text{C}$ observations shown in Fig. 10.

3.3. The $^{14}\text{C}/^{12}\text{C}$ Transient Centred at about 12,000 cal-yr-BP

The paleomagnetic (McElhinny and Senanayake, 1982; Guyodo and Valet, 1996; Fig. 8) and the ^{10}Be records (Yiou et al., 1998; Finkel and Nishiizumi, 1998) do not exhibit a significant transient that could explain the atmospheric ^{14}C excursion centered at between 13,000 and 12,000 cal-yr-BP (Figs. 12, 13). As proposed by Oeschger et al. (1980), Goslar et al. (1995), and Hughen et al. (1998), major changes in the rate of exchange within the carbon cycle must have caused this millenium-scale event which occurred during the Younger Dryas (YD) cold period (Fig. 13). Using box models, these authors suggested that an abrupt slow-down of the North-Atlantic deep water (NADW) convection was responsible for the early rise of atmospheric $\Delta^{14}\text{C}$ at about 13,000 cal-yr-BP associated with the initial cooling of the YD event. Based on a detailed dataset from the Cariaco basin varves, Hughen et al. (1998) showed that the atmospheric $\Delta^{14}\text{C}$ began its subsequent decrease during and not at the end of the YD. As explained by Hughen et al. (1998) and Broecker (1998), this paradox could be explained if the excess atmospheric ^{14}C was sucked up by other parts of the ocean which have less influence on the global climate than the North Atlantic area of deep convection.

Inherent to their box-modelling approach, Goslar et al. (1995) and Hughen et al. (1998) make ad hoc assumptions about the timing of the oceanic convection changes. By using physically realistic models, Stocker and Wright (1996) and Mikolajewicz (1996) attempted to calculate simultaneously the oceanographic and climatic changes during the YD and the concomitant atmospheric $\Delta^{14}\text{C}$ maximum. In both of these modelling studies, the initial cause of all these variations is the dramatic increase in the flux of deglacial freshwater known as meltwater pulse 1A (MWP1A; Fairbanks, 1989; Bard et al., 1990b, 1996; Fig. 14). This major climatic event corresponds to an abrupt sea-level rise at a mean rate of 4–5 m per century over a period of about 400 yr. This is equivalent to an annual melting of about $16,000 \text{ km}^3$ of continental ice and to an increase by 0.5 Sv of the freshwater flux into the Atlantic ($1\text{Sv} = 10^6 \text{ m}^3 \cdot \text{s}^{-1}$). The main effect of this massive injection of freshwater in the North-Atlantic is to reduce abruptly the

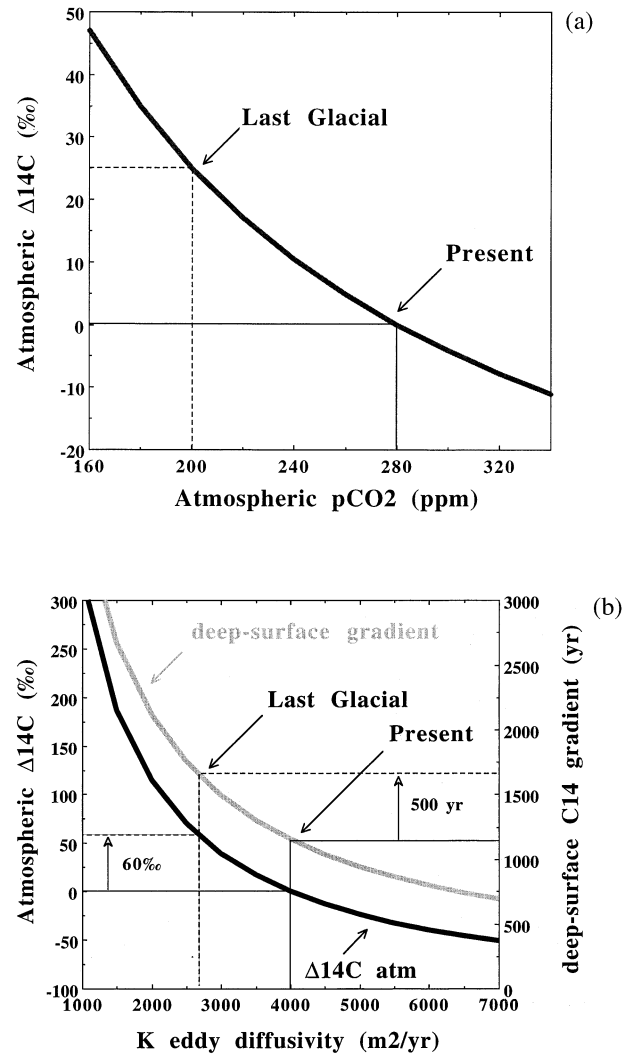


Fig. 11. Variations of atmospheric $\Delta^{14}\text{C}$ expected from carbon cycle changes. These theoretical curves represent equilibrium values computed by means of a box-diffusion model (Oeschger et al., 1975). The upper panel (11a) shows that the atmospheric $\Delta^{14}\text{C}$ increases when atmospheric pCO_2 decreases. As shown by studies of air bubbles in ice cores (Delmas et al., 1980; Neftel et al., 1982), the glacial pCO_2 was 80 ppm lower than the present-day natural value (ca. 280 ppm). This pCO_2 change alone was probably accompanied by a $\Delta^{14}\text{C}$ increase by ca. 25‰ (see also Siegenthaler, 1980 and Lal and Revelle, 1984 for similar estimates). This value is probably a lower bound since several authors have shown that the biospheric reservoir was also reduced during the glacial period (Adams et al., 1990; Van Campo et al., 1993; Crowley, 1995). The lower panel (11b) shows the effect of changes of deep-sea ventilation parameterized with a single eddy diffusivity coefficient in the model (K in m^2yr^{-1}). The present-day K value is $4000 \text{ m}^2\text{yr}^{-1}$ which leads to an average ^{14}C gradient of ca. 1150 yr between surface and deep sea (grey curve associated with the right-hand y-axis). AMS- ^{14}C data on contemporaneous benthic and planktonic foraminifera (Broecker et al., 1984) indicate that this gradient was larger during the glacial period (Shackleton et al., 1988; Broecker et al., 1990). For simplicity, an increase of this ^{14}C gradient by 500 yr was assumed for the glacial period which can be produced with a reduced value of K ($2665 \text{ m}^2\text{yr}^{-1}$). This sluggish ventilation is responsible for an increase of ca. 60‰ in the atmospheric $\Delta^{14}\text{C}$ (black curve associated to the left-hand y-axis).

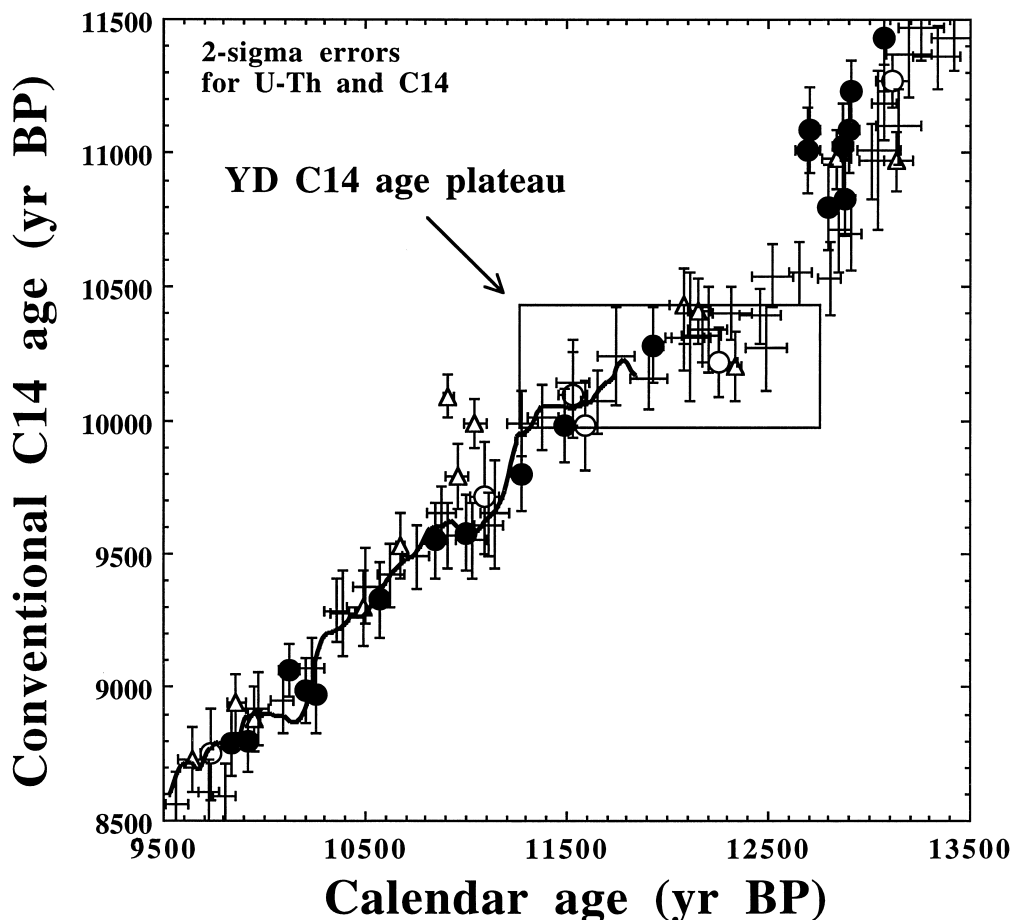


Fig. 12. (Detail of Fig. 1b): AMS- ^{14}C ages plotted vs. TIMS- ^{230}Th ages obtained on corals. Open dots represent the coral data from Barbados, black dots the coral data from Tahiti (Bard et al., 1990, 1993, 1996 and 1998), open triangles the coral data from New Guinea (Edwards et al., 1993) and crosses the foraminifera data obtained on varved marine sediments from the Cariaco basin (Hughen et al., 1998). Statistical errors for coral and foraminifera data are quoted at the 2σ level. The wiggly curve is the smoothed tree-ring calibration (Kromer and Spurk, 1998). Note the excellent agreement between the different datasets in this narrow time range. The box indicates a millenium-long period during which ^{14}C ages are almost constant (Oeschger et al., 1980). This is often referred as the major ^{14}C age plateau which occurred during the Younger Dryas cold period.

formation of NADW (Fig. 15). The strong reduction in NADW formation had a direct influence on the atmospheric $\Delta^{14}\text{C}$ (Figs. 16, 17) and on the climate of high-latitudes in the North Atlantic and European sectors (Fig. 17)

When compared to box modelling simulations, the GCM approach is certainly a major improvement but a puzzling problem remains to be solved: the relative timing of simulated $\Delta^{14}\text{C}$ variations and climatic changes disagrees with the observations. The data demonstrate that the atmospheric $\Delta^{14}\text{C}$ and climatic excursions (i.e., start of YD) began in phase (Fig. 13) but about a millenium later than MWP1A, that was centred at about 14,000 cal-yr-BP (Fig. 14). By contrast, the numerical simulations summarized on Figs. 16 and 17 suggest essentially no time lag between the meltwater discharge and its effects on climate and atmospheric $\Delta^{14}\text{C}$ (Stocker and Wright, 1996; Mikolajewicz, 1996).

3.3. The Older Part of the Calibration and its Relationship with the ^{10}Be Peak

Between 30,000 and 45,000 yr BP (practical limit of the ^{14}C method) the calibration curve suffers mainly from a lack of accurate data. Bard et al. (1998) analysed a single coral sample collected from the lower uplifted terrace from Huon Peninsula, Papua New Guinea, previously dated by TIMS U-Th at $41,100 \pm 500$ cal-yr-BP (Dia et al., 1993). The discrepancy between the ^{14}C and U-Th age is about 5500 yr (Fig. 1), also corresponding to a surprisingly high $\Delta^{14}\text{C}$ of ca. 700‰. For such an old sample, the diagenetic alteration and ^{14}C chemistry blank are critical problems, and this data on an isolated coral is tentative and needs to be replicated. However, it is worth pointing out that similar age shifts of the order of 5000 yr have been obtained by comparing mass spectrometric ^{14}C and U-Th ages

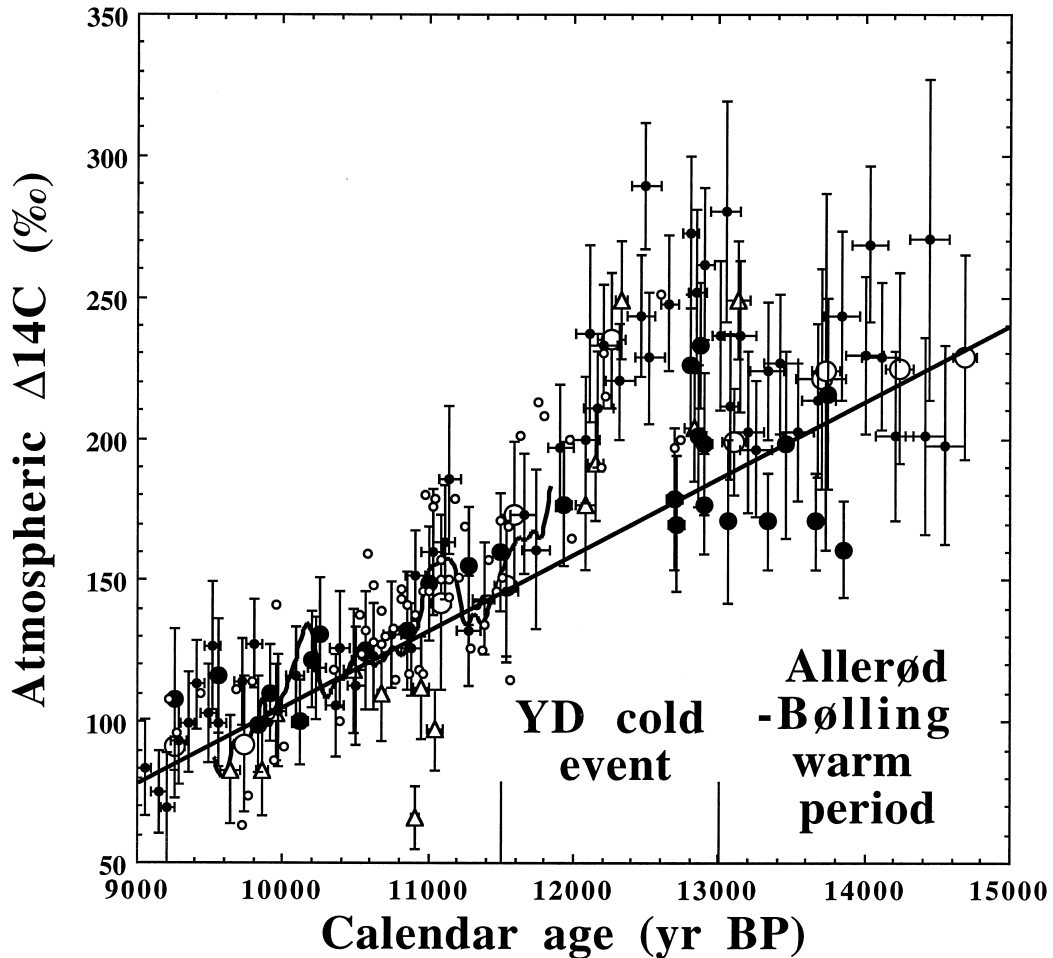


Fig. 13. (Detail of Fig. 2). Large open dots represent the coral data from Barbados, black dots the coral data from Tahiti (Bard et al., 1990, 1993, 1996 and 1998), open triangles the coral data from New Guinea (Edwards et al., 1993), small open dots the data obtained on varved sediments from Lake Gosciuz (Goslar et al., 1995) and crosses the data obtained on varved marine sediments from the Cariaco basin (Hughen et al., 1998; Lin et al., 1997). Statistical errors for coral and foraminiferal data are quoted at the 2σ level. For the sake of clarity, no error bars are shown for the Gosciuz data (see Goslar et al., 1995 for details). The wiggly curve is the smoothed German pine calibration (Kromer and Spurk, 1998). The black thick line approximates the long term trend of atmospheric $\Delta^{14}\text{C}$ which is probably due to a slow decrease of the ^{14}C production (see text). Note the ca. 50‰ excursion centred at about 12,500 cal-yr-BP which roughly corresponds to the Younger Dryas cold event (13,000–11,500 cal-yr-BP). The abrupt $\Delta^{14}\text{C}$ decrease between 12,500 and 11,500 cal-yr-BP is responsible for the major ^{14}C age plateau seen on Fig. 12.

measured in an archeological site (Bishoff et al., 1994). In addition, Vogel and Kronfeld (1997) applied conventional radioactive counting techniques to date old stalagmites from South Africa by U-Th and ^{14}C . Although the reliability of ^{14}C and U-Th ages in speleothems is not as high as for corals (problems of unknown or variable initial ^{14}C age and detrital Th contamination in speleothems), the main outcome of the work by Vogel and Kronfeld (1997) is that ^{14}C dates between 35,000 and 45,000 cal-yr-BP are indeed 5000 yr too young. Large differences between ^{14}C and TIMS U-Th ages were also obtained recently on lacustrine inorganic aragonite (Schramm et al., 1996) and on speleothems from the Bahamas (Richards et al., 1997).

These five independent works comparing ^{14}C and U-Th ages are in apparent contrast with the atmospheric $\Delta^{14}\text{C}$ recon-

structed by using varved sediments from a Japanese lake (Kitagawa and van der Plicht, 1998). However, as acknowledged by these authors, their varve counts between 20,000 and 38,000 cal-yr-BP should be considered as minimum ages due to the high probability of missing varves. Furthermore, beyond 38,000 cal-yr-BP, the $\Delta^{14}\text{C}$ record from the Japanese lake is only based on an extrapolation of the sedimentation rate and not on true annual counts (see Figs. 1a and 3 in Kitagawa and van der Plicht, 1998).

This 35,000–45,000 cal-yr-BP interval was a troubled one for cosmogenic isotopes because it encompasses the Laschamp geomagnetic excursion (Bonhommet and Zähringer, 1969; Hall and York, 1978; Gillot et al., 1979; Levi et al., 1990) and includes prominent and concomitant ^{10}Be and ^{36}Cl maxima first revealed in polar ice (Raisbeck et al., 1987; Beer et al.,

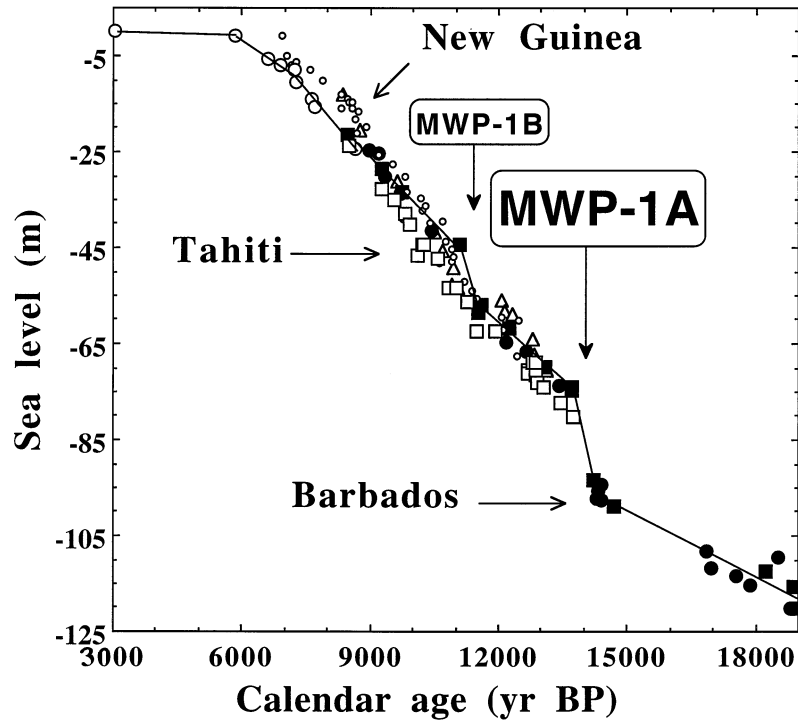


Fig. 14. Sea-level variation history reconstructed for long drill cores from Barbados (black squares and circles), Tahiti (large open squares and circles), and New Guinea (open triangles and small open circles). For clarity, samples dated by ^{14}C only were converted to calendar years by means of calibration formulae (Bard et al., 1993) and are indicated by circular symbols. The sea-level curves based on U-Th ages can be found in the following references: Bard et al. (1990b) for Barbados, Edwards et al. (1993) for New Guinea and Bard et al. (1996) for Tahiti. The sea-level curves based on ^{14}C ages can be found in the following references: Fairbanks (1989) for Barbados, Chappell and Polach (1991) for New Guinea, and Bard et al. (1996) for Tahiti. Local vertical movements were corrected for the different sites; the small but systematic shifts could be attributed to different hydro-isostatic responses for the three islands. Arrows indicate the median ages of MWP-1A and MWP-1B, first revealed in the case of Barbados (Fairbanks, 1989; Bard et al., 1990).

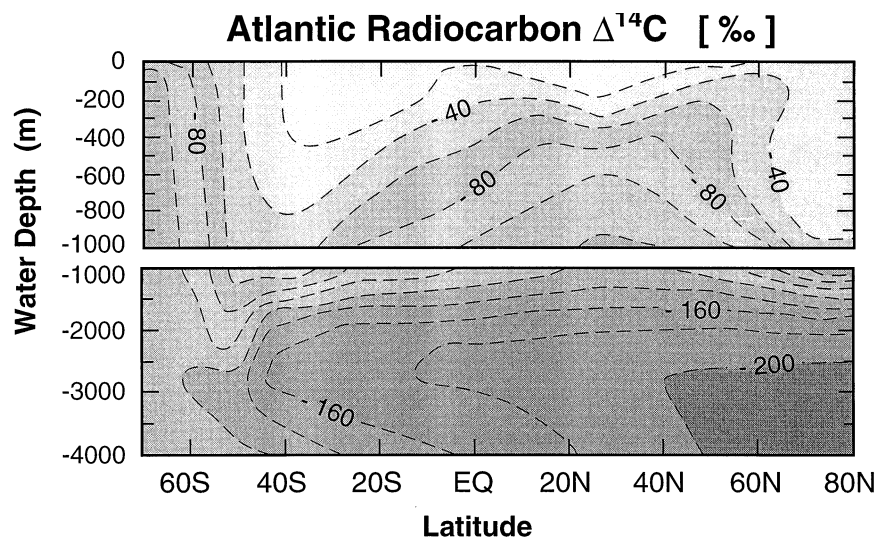


Fig. 15. $\Delta^{14}\text{C}$ isolines of dissolved inorganic carbon for the Atlantic Ocean after the injection of MWP-1A (after Stocker and Wright, 1996). The North Atlantic overturning is in a collapsed state and this cross-section is similar to the present-day Pacific (note the very low $\Delta^{14}\text{C}$ values at 3 km depth between 50 and 80°N).

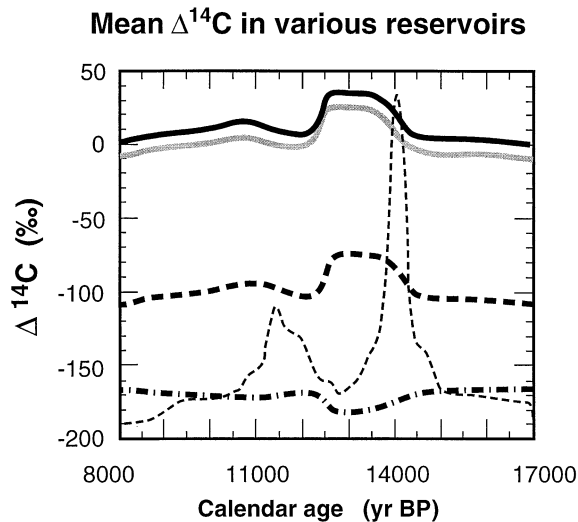


Fig. 16. Evolution of mean $\Delta^{14}\text{C}$ in the major reservoirs of the carbon cycle perturbed by meltwater injection during the last deglaciation (after Stocker and Wright, 1996). The thin dashed line represents the Barbados meltwater record taken as the first derivative of the Barbados sea level curve (Fig. 14). The black curve refers to the atmosphere, the grey curve to the biosphere, the dashed curve to the upper 1000 m of the ocean and the dashed-dotted curve to the deeper ocean. The atmospheric $\Delta^{14}\text{C}$ increases by up to 35‰ which agrees with simpler box model calculations (Goslar et al., 1995).

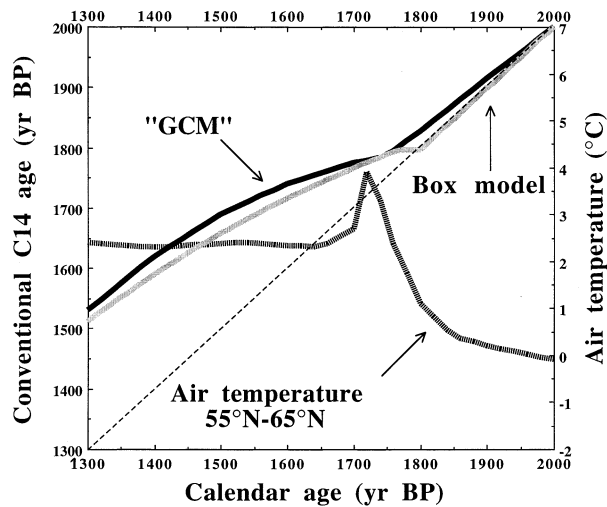


Fig. 17. Simulation of a ^{14}C age plateau by numerical models: the black line corresponds to the coupled global ocean-ice-atmosphere-biosphere (GCM) model of Stocker and Wright (1996) and the grey line to the twelve-box model of Bard et al. (1997). The GCM model is perturbed by meltwater injection during the last deglaciation. The ^{14}C age plateau occurs when the North-Atlantic overturning is restored, which also corresponds to an abrupt warming of the northern troposphere at high-latitudes (dotted curve associated with right axis). In the box model experiment, the ^{14}C age plateau begins when NADW formation is restored from a reduced state (10 Sv) to a modern rate (20 Sv). As explained in the text, there is a puzzling problem concerning the relative timing of climatic and ^{14}C changes. Hence, the start of the ^{14}C age plateau is set arbitrarily at about 1800 yr BP. Note, however, that the simulated age plateau is significantly shorter than the real plateau shown in Fig. 12.

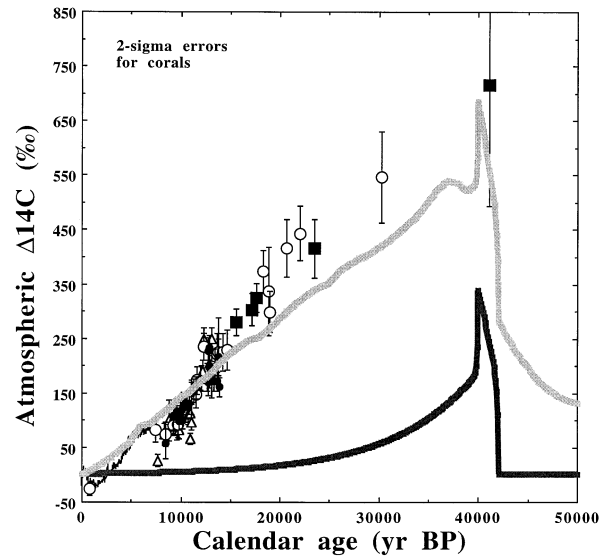


Fig. 18. Atmospheric $\Delta^{14}\text{C}$ vs. time as calculated by using the AMS- ^{14}C ages vs. TIMS- ^{230}Th comparison. Statistical errors for coral data are quoted at the 2σ level. Open dots represent the data from Barbados, black dots the data from Tahiti, black squares with small errors the data from Mururoa (Bard et al., 1990, 1993, 1996 and 1998) and open triangles the data from New Guinea (Edwards et al., 1993). The oldest black square at ca. 41,100 cal-yr-BP with a large error corresponds to sample KWA-I-1 collected in the lower uplifted terrace of Huon Peninsula, Papua New Guinea. The thick black curve shows the atmospheric $\Delta^{14}\text{C}$ expected as a response to a doubling of the cosmnuclide production between 42,000 and 40,000 cal-yr-BP, the time of the major ^{10}Be peak. This production scenario was used as an input for a simple carbon cycle box-model used in Bard et al. (1990). In a similar way, the thick grey curve was obtained by assuming that this doubling of the production is superimposed on geomagnetic intensity variations as compiled by Guyodo and Valet (1996; see Fig. 8).

1992; Yiou et al., 1997; Baumgartner et al., 1998). This ^{10}Be - ^{36}Cl peak corresponds approximately to a doubling of the flux over a period of about 2000 yr which occurred at about 41,000 cal-yr-BP as dated in Greenland ice (Yiou et al., 1997; Finkel and Nishiizumi, 1996, 1997). A preliminary explanation for the ^{10}Be - ^{36}Cl peak could be a direct causal link with the Laschamp excursion during which the magnetic field fell drastically in intensity (Levi et al., 1990; Baumgartner et al., 1998). This explanation remains hypothetical and other causes have been invoked such as an extreme solar modulation (Raisbeck et al., 1987), the shockwave of a supernova explosion (Sonett et al., 1987) or even the fortuitous combination of several of these causes (McHargue et al., 1995; Robinson et al., 1995).

Simulating the atmospheric $\Delta^{14}\text{C}$ for the 35,000–45,000 cal-yr-BP period is not an easy task because the geodynamo was probably not dipolar during the Laschamp event and because the magnitude of ^{14}C changes associated with the ^{10}Be - ^{36}Cl peak depends on its causes which are still hypothetical. As a working hypothesis, I assumed that the ^{10}Be - ^{36}Cl doubling seen in polar ice cores is due to a solar effect superimposed on slow variations of the geomagnetic field. The resulting simulation suggests that the combination of these effects could

explain the very elevated atmospheric $\Delta^{14}\text{C}$ in excess of 500‰ over a duration of 10,000 yr (Fig. 18).

4. CONCLUSIONS

Significant variations of the atmospheric $^{14}\text{C}/^{12}\text{C}$ ratio have been caused by a variety of geophysical, climatological, and astrophysical causes: (1) Most short term ^{14}C excursions occurring over the time scale of centuries are linked to cosmic-ray modulation by the magnetic properties of the solar wind. (2) The long-term $\Delta^{14}\text{C}$ decrease during the last 30,000 cal-yr-BP is clearly a response to a slow increase of the intensity of the Earth magnetic dipole. (3) In addition to ^{14}C production variations, the atmospheric $\Delta^{14}\text{C}$ was also affected by internal changes within the carbon cycle. In particular, the so-called ^{14}C age plateaux are probably linked to abrupt changes in oceanic ventilation which occurred during the last deglaciation.

More work is still needed to supplement our knowledge of the variations of the atmospheric $\Delta^{14}\text{C}$ ratio, especially for the time period between 30,000 and 45,000 cal-yr-BP. In order to make significant advances in understanding the causes of atmospheric $\Delta^{14}\text{C}$ variations, it is highly desirable to obtain new datasets for other cosmogenic nuclides from records spread over different latitudes as well as new $\Delta^{14}\text{C}$ data from other reservoirs of the carbon cycle, in particular from the deep and intermediate ocean by analysing benthic foraminifera and deep sea corals (e.g., Mangini et al., 1998; Adkins et al., 1998).

Acknowledgements—I thank Drs. M. Arnold, T. Goslar, B. Hamelin, G. Raisbeck, and F. Yiou for fruitful collaborations and discussions over the last 10 years, Dr. D. Bourlès for review of the manuscript, Dr. B. Kromer for early release of data, J. J. Motte for drawing, and Dr. M. S. N. Carpenter for correcting the English style. This work was supported by IUF, CNRS, and EC grants.

REFERENCES

- Adams J. M., Faure H., Faure-Denard L., McGlade J. M., and Woodward F. I. (1990) Increases in terrestrial carbon storage from the last glacial maximum to the present. *Nature* **348**, 711–714.
- Adkins J. F., Cheng H., Boyle E. A., Druffel G. R. M., and Edwards R. L. (1998) Deep-sea coral evidence for rapid change in ventilation of the deep North Atlantic 15,400 years ago. *Science* **280**, 725–728.
- Andree M. et al. (1984) ^{14}C measurements on foraminifera of deep-sea core V28-238 and their preliminary interpretation. *Nucl. Inst. Meth. Phys. Res.* **B5**, 340–345.
- Baliunas S. and Jastrow R. (1990) Evidence for long-term brightness changes of solar-type stars. *Nature* **348**, 520–522.
- Bard E., Arnold M., Maurice P., Duprat J., Moyes J., and Duplessy J. C. (1987) Retreat velocity of the North-Atlantic polar front during the last deglaciation determined by ^{14}C accelerator mass spectrometry. *Nature* **328**, 791–794.
- Bard E., Hamelin B., Fairbanks R. G., and Zindler A. (1990a); Calibration of ^{14}C timescale over the past 30,000 years using mass spectrometric U-Th ages from Barbados corals. *Nature* **345**, 405–410.
- Bard E., Hamelin B., and Fairbanks R. G. (1990b) U/Th ages obtained by mass spectrometry in corals from Barbados: Sea level during the past 130,000 years. *Nature* **346**, 456–458.
- Bard E., Arnold M., Fairbanks R. G., and Hamelin B. (1993) $^{230}\text{Th}/^{234}\text{U}$ and ^{14}C ages obtained by mass spectrometry on corals. *Radiocarbon* **35**, 191–199.
- Bard E. et al. (1996) Deglacial sea level record from Tahiti corals and the timing of global meltwater discharge. *Nature* **382**, 241–244.
- Bard E., Raisbeck G., Yiou F., and Jouzel J. (1997) Solar modulation of cosmogenic nuclide production over the last millennium: Comparison between ^{14}C and ^{10}Be records. *Earth Planet. Sci. Lett.* **150**, 453–462.
- Bard E., Arnold M., Hamelin B., Tisnerat-Laborde N., and Cabioch G. (1998) Radiocarbon calibration by means of mass spectrometric $^{230}\text{Th}/^{234}\text{U}$ and ^{14}C ages of corals: An updated data base including samples from Barbados, Mururoa and Tahiti. *Radiocarbon* (in press).
- Baumgartner S., Beer J., Masarik J., Wagner G., Meynadier L., and Synal H.-A. (1998) Geomagnetic modulation of the ^{36}Cl flux in the GRIP ice core, Greenland. *Science* **279**, 1330–1332.
- Beer J. et al. (1988) Information on past solar activity and geomagnetism from ^{10}Be in the Camp Century ice core. *Nature* **331**, 675–679.
- Beer J. et al. (1992) ^{10}Be peaks as time markers in polar ice cores. In *The Last Deglaciation: Absolute and Radiocarbon Chronologies* (ed. E. Bard and W. S. Broecker); NATO ASI Ser. I, **2**, 141–153. Springer Verlag.
- Bennett C. L. et al. (1977) Radiocarbon dating using electrostatic accelerators: Negative ions provide the key. *Science* **198**, 508–510.
- Bonhommet N. and Zähringer J. (1969) Paleomagnetism and potassium argon determinations of the Laschamp geomagnetic polarity event. *Earth Planet. Sci. Lett.* **6**, 43–46.
- Bischoff J. L. et al. (1994) Dating of the basal aurignacian sandwich at Abric Romani (Catalunya, Spain) by radiocarbon and uranium-series. *J. Archaeol. Sci.* **21**, 541–551.
- Broecker W. S. (1998) Paleocirculation during the last deglaciation: A bipolar seesaw? *Paleoceanography* **13**, 119–121.
- Broecker W. S. and Olson E. A. (1961) Lamont radiocarbon measurements VIII. *Radiocarbon* **3**, 176–204.
- Broecker W. S., Mix A., Andree M., and Oeschger H. (1984) Radiocarbon measurements on coexisting benthic and planktic foraminifera shells: Potential for reconstructing ocean ventilation times over the 20000 years. *Nucl. Inst. Meth. Phys. Res.* **B5**, 331–339.
- Broecker W. S., Peng T.H., Trumbore S., Bonani G., and Wölflfi W. (1990) The distribution of radiocarbon in the glacial ocean. *Global Biogeochemical Cycles* **4**, 103–117.
- Campbell W. H. (1997) *Introduction to Geomagnetic Fields*. Cambridge Univ. Press.
- Chappell J. and Polach H. (1991) Post-glacial sea-level rise from a coral record at Huon Peninsula, Papua New-Guinea. *Nature* **349**, 147–149.
- Craig H. (1957) The natural distribution of radiocarbon and the exchange time of carbon dioxide between the atmosphere and sea. *Tellus* **9**, 1–17.
- Crowley T. J. (1995) Ice age terrestrial carbon changes revisited. *Global Biogeochemical Cycles* **9**, 377–389.
- Delmas R. J., Ascencio J. M., and M. Legrand M. (1980) Polar ice evidence that atmospheric CO_2 29,000 years B.P. was 50% of the present. *Nature* **284**, 155–157.
- deMairan J. J. D. (1733) *Traité Physique et Historique De L'aurore Boréale*. Imprimerie Royale.
- deVries H. L. (1958) Variation in concentration of radiocarbon with time and location on Earth. *Proc. Koninkl. Ned. Akad. Wetenschap.*, 94–102.
- Dia A. N., Cohen A. S., O'Nions R. K., and Shackleton N. J. (1993) Seawater Sr isotope variation over the past 300 kyr and influence of global climate cycles. *Nature* **365**, 786–788.
- Duplessy J. C., Arnold M., Maurice P., Bard E., Duprat J., and Moyes J. (1986) Direct dating of the oxygen-isotope record of the last deglaciation by ^{14}C accelerator mass spectrometry. *Nature* **320**, 350–352.
- Eddy J. A. (1976) The Maunder minimum. The reign of Louis XIV appears to have been a time of real anomaly in the behavior of the sun. *Science* **192**, 1189–1202.
- Edwards R. L., Chen J. H., and Wasserburg G. J. (1987) ^{238}U - ^{234}U - ^{230}Th - ^{232}Th systematics and the precise measurement of time over the past 500,000 yrs. *Earth Planet. Sci. Lett.* **81**, 175–192.
- Edwards R. L. et al. (1993) A large drop in atmospheric $^{14}\text{C}/^{12}\text{C}$ and reduced melting in the Younger Dryas, documented with ^{230}Th ages of corals. *Science* **260**, 962–968.
- Elsasser W., Ney E. P., and Winckler J. R. (1956) Cosmic-ray intensity and geomagnetism. *Nature* **178**, 1226–1227.
- Fairbanks R. G. (1989) A 17,000-year glacio-eustatic sea level record:

- Influence of glacial melting rates on the Younger Dryas event and deep ocean circulation. *Nature* **342**, 637–647.
- Finkel R. C. and Nishiizumi K. (1996) ^{10}Be and ^{36}Cl concentrations in the GISP2 ice core compared with $\Delta^{14}\text{C}$ in tree rings. Abstract of AGU Fall Meeting, *EOS* **77**, F428 (abstr.).
- Finkel R. C. and Nishiizumi K. (1997) ^{10}Be concentrations in the GISP2 ice core from 3 to 40 ky. *J. Geophys. Res.* **102**, 26,699–26,782.
- Frank M., Schwarz B., Baumann S., Kubik P. W., Suter M., and Mangini A. (1997) A 200 kyr record of cosmogenic radionuclide production rate and geomagnetic field intensity from ^{10}Be in globally stacked deep-sea sediments. *Earth Planet. Sci. Lett.* **149**, 121–130.
- Gillot P. Y. et al. (1979) Age of the Laschamp paleomagnetic excursion revisited. *Earth Planet. Sci. Lett.* **42**, 444–450.
- Goslar T. et al. (1995) High concentration of atmospheric ^{14}C during the Younger Dryas cold episode. *Nature* **377**, 414–417.
- Guyodo Y. and Valet J.-P. (1996) Relative variations in geomagnetic intensity from sedimentary records: The past 200,000 years. *Earth Planet. Sci. Lett.* **143**, 23–36.
- Hall C. M. and York D. (1978) K-Ar and $^{40}\text{Ar}/^{39}\text{Ar}$ age of the Laschamp geomagnetic polarity reversal. *Nature* **274**, 462–464.
- Hughen K. A. et al. (1998) Deglacial changes in ocean circulation from an extended radiocarbon calibration. *Nature* **391**, 65–68.
- Kitagawa H. and van der Plicht J. (1998) Atmospheric radiocarbon calibration to 45,000 yr BP: Late glacial fluctuations and cosmogenic isotope production. *Science* **279**, 1187–1190.
- Kromer B. and Becker B. (1993) German oak and pine ^{14}C calibration, 7200 BC to 9439 BC. *Radiocarbon* **35**, 125–135.
- Kromer B. and Spurk M. (1998) Revision and tentative extension of the tree-ring ^{14}C calibration 9200 to 11900 Cal BP. *Radiocarbon* (in press).
- Lal D. (1988) Theoretically expected variations in the terrestrial cosmic-ray production rates of isotopes. In *Solar-Terrestrial Relationships and the Earth Environment in the Last Millennia* (ed. X. C. V. Corso), pp. 216–233. Soc. Italiana di Fisica
- Lal D. and Revelle R. (1984) Atmospheric PCO_2 changes recorded in lake sediments. *Nature* **308**, 344–346.
- Lao Y., Anderson R.F., Broecker W. S., Trumbore S. E., Hofmann H. J., and Wölfli W. (1992) Increased production of cosmogenic ^{10}Be during the Last Glacial Maximum. *Nature* **357**, 576–578.
- Levi S., Audunsson H., Duncan R. A., Kristjanson L., Gillot P. Y., and Jakobsson S. P. (1990) Late Pleistocene geomagnetic excursion in Icelandic lavas: Confirmation of the Laschamp excursion. *Earth Planet. Sci. Lett.* **96**, 443–457.
- Libby W. F. (1952) *Radiocarbon Dating*. Univ. Chicago Press.
- Lin et al. (1997) Late Quaternary climate change from $\delta^{18}\text{O}$ records of multiple species of planktonic foraminifera: High-resolution records from the anoxic Cariaco Basin, Venezuela. *Paleoceanography* **12**, 415–427.
- Lockwood G. W., Skiff B. A., Baliunas S. L., and Radick R. R. (1992) Long-term solar brightness changes estimated from a survey of Sun-like stars. *Nature* **360**, 653–655.
- Mangini A. et al. (1998) Coral provides way to age deep water. *Nature* **392**, 347
- Maunder R. W. (1894) A prolonged sunspot minimum. *Knowledge* **17**, 173–176.
- McElhinny M. W. and Senanayake W. E. (1982) Variations in the geomagnetic dipole I: the past 50,000 years. *J. Geomagnet. Geoelectr.* **34**, 39–51.
- McHargue L. R., Damon P. E., and Donahue D. J. (1995) Enhanced cosmic-ray production of ^{10}Be coincident with the Mono Lake and Laschamp geomagnetic excursions. *Geophys. Res. Lett.* **22**, 659–662.
- Mikolajewicz U. (1996) A meltwater induced collapse of the conveyor belt thermohaline circulation and its influence on the distribution of $\Delta^{14}\text{C}$ and $\delta^{18}\text{O}$ in the oceans. *Max-Planck-Inst. Meteor. Rep.* **189**, 1–25.
- Monaghan M. C., Krishnaswami S., and Turekian K. K. (1985) The global average production rate of ^{10}Be . *Earth Planet. Sci. Lett.* **76**, 279–287.
- Neftel A., Oeschger H., Swander J., Stauffer B., and Zimbrunn R. (1982) Ice core sample measurements give atmospheric CO_2 content during the past 40,000 years. *Nature* **295**, 220–223.
- Nelson D. E., Korteling R. G., and Stott W. R. (1977) Carbon-14: Direct detection at natural levels. *Science* **198**, 507–508.
- Oeschger H., Siegenthaler U., Schotterer U., and Gugelmann A. (1975) A box diffusion model to study the carbon dioxide exchange in nature. *Tellus* **27**, 168–192.
- Oeschger H. et al. (1980) ^{14}C and other parameters during the Younger Dryas cold phase. *Radiocarbon* **22**, 299–310.
- Plummer M. A., Phillips F. M., Fabryka-Martin J., Turin H. J., Wigand P. E., and Sharma P. (1997) Chlorine-36 in fossil rat urine: An archive of cosmogenic nuclide deposition during the past 40,000 years. *Science* **277**, 538–541.
- Raisbeck G. M. et al. (1981) Cosmogenic ^{10}Be concentrations in Antarctic ice during the past 30,000 years. *Nature* **292**, 825–826.
- Raisbeck G. M., Yiou F., Bourles D., Lorius C., Jouzel J., and Barkov N. I. (1987) Evidence for two intervals of enhanced ^{10}Be deposition in Antarctic ice during the last glacial period. *Nature* **326**, 273–277.
- Raisbeck G. M., Yiou F., Jouzel J., Petit J. R., Barkov N. I., and Bard E. (1992) ^{10}Be deposition at Vostok, Antarctica, during the last 50,000 years and its relationship to possible cosmogenic production variations during this period. In *The Last Deglaciation: Absolute and Radiocarbon Chronologies* (ed. E. Bard and W. S. Broecker); NATO ASI Ser. I, **2**, 127–140. Springer-Verlag.
- Richards D. A., Beck J. W., Burr G. S., Donahue D. J., Smart P. L., and Edwards R. L. (1997) Calibration of radiocarbon timescale from 13 to 50 ka using C-14 and Th-230 ages of speleothems from the Bahamas. Abstract of AGU Fall Meeting, *EOS* **78**, F389 (abstr.).
- Robinson C., Raisbeck G. M., Yiou F., Lehman B., and Laj C. (1995) The relationship between ^{10}Be and geomagnetic field strength records in central North Atlantic sediments during the last 80 ka. *Earth Planet. Sci. Lett.* **136**, 551–557.
- Schramm A., Stein M., and Goldstein S. L. (1996) U-series and ^{14}C dating of Lake Lisan (Paleo-Dead Sea) sediments: Implications for ^{14}C time-scale calibration and relation to global paleoclimate. Abstract of AGU Fall Meeting, *EOS* **77**, F303–304. (abstr.).
- Shackleton N. J., Duplessy J. C., Arnold M., Maurice P., Hall M. A., and Cartlidge J. (1988) Radiocarbon age of the last glacial deep water. *Nature* **335**, 708–711.
- Siegenthaler U., Heimann M., and Oeschger H. (1980) ^{14}C variations caused by changes in the global carbon cycle. *Radiocarbon* **22**, 177–191.
- Sonett C. P., Morfill G. E., and Jokipii J. R. (1987) Interstellar shock waves and ^{10}Be from ice cores. *Nature* **330**, 458–460.
- Stocker T. F. and Wright D. G. (1996) Rapid changes in ocean circulation and atmospheric radiocarbon. *Paleoceanography* **11**, 773–795.
- Stuiver M. (1961) Variations in radiocarbon concentration and sunspot activity. *J. Geophys. Res.* **66**, 273–276.
- Stuiver M. and Polach H. A. (1977) Reporting of C14 data. *Radiocarbon* **19**, 355–363.
- Stuiver M. and Quay P. D. (1980) Changes in atmospheric carbon-14 attributed to a variable sun. *Science* **207**, 11–19.
- Stuiver M., Kromer B., Becker B., and Ferguson C. W. (1986) Radiocarbon age calibration back to 13,300 years BP and the ^{14}C age matching of the German oak and US bristlecone pine chronologies. *Radiocarbon* **28**, 969–979.
- Stuiver M. and Reimer P. J. (1993) Calib Rev. 3. *Radiocarbon* **35**, 215–230.
- Svensmark H. and Friis-Christensen E. (1997) Variations of cosmic ray flux and global cloud coverage—a missing link in solar-climate relationships. *J. Atmos. Solar-Terrest. Phys.* **59**, 1225–1232.
- Tauxe L. (1993) Sedimentary record of relative paleointensity of the geomagnetic field: Theory and practice. *Rev. Geophys.* **31**, 319–354.
- Thouveny N., Creer K., and Williamson D. (1993) Geomagnetic moment variations in the last 70 kyr, impact on production of cosmogenic isotopes. *Global Planetary Change* **7**, 157–172.
- Tinsley B. A. (1994) Solar wind mechanism suggested for weather and climate change. *EOS Transactions*, **75**, 369–374.
- Tric E. et al. (1992) Paleointensity of the geomagnetic field during the last 80,000 years. *J. Geophys. Res.* **97**, 9337–9351.

- Van Campo E., Guiot J., and Peng C. (1993) A data-based reappraisal of the terrestrial carbon budget at the last glacial maximum. *Global Planetary Change* **8**, 189–201.
- Vogel J. C. and Kronfeld J. (1997) Calibration of radiocarbon dates for the late Pleistocene using U/Th on stalagmites. *Radiocarbon* **39**, 27–32.
- Yiou F. et al. (1997) ^{10}Be in the GRIP ice core at Summit, Greenland. *J. Geophys. Res.* **102**, 26,783–26,794.
- Zhang Q., Soon W.H., Baliunas S. L., Lockwood G. W., Skiff B. A., and Radick R. R. (1994) A method of determining possible brightness variations of the sun in past centuries from observations of solar-type stars. *Astrophys. J.* **427**, L111–L114.